JACS
JOURNAL OF THE AMERICAN CHEMICAL SOCIETY
Communication
pubs.acs.org/JACS

Quick, Controlled Synthesis of Ultrathin Bi_2Se_3 Nanodiscs and Nanosheets

Yuho Min,[†,§] Geon Dae Moon,[†,§] Bong Soo Kim,[†] Byungkwon Lim,[‡] Jin-Sang Kim,[∥] Chong Yun Kang,[∥] and Unyong Jeong*,[†]

[†]Department of Materials Science and Engineering, Yonsei University, 134 Shinchon-dong, Seoul, Korea
[‡]School of Advanced Materials Science and Engineering, Sungkyunkwan University, Suwon 440-746, Korea
[∥]Electronic Materials Research Center, KIST, Seoul, Korea

Ⓢ *Supporting Information*

ABSTRACT: Ultrathin (4−6 nm) single-crystal Bi_2Se_3 nanodiscs and nanosheets were synthesized through a simple and quick solution process. The growth mechanism was investigated in detail. Crystal seeds grew via 2D self-attachment of small nanoparticles followed by epitaxial recrystallization into single crystals. The lateral dimension of the nanodiscs increased and their shape changed from circles to hexagons as the reaction temperature increased. Positively charged polymer surfactants greatly enlarged the lateral dimension to produce nanosheets with uniform thickness.

Characteristics of topological insulators have been theoretically predicted and experimentally observed in Bi chalcogenides.[1−4] Topological insulator thin films possess special surface states that fall within the bulk energy gap. The unusual conductive metallic surfaces are expected to afford new spintronic devices at room temperature.[4] Bi_2Se_3 has received interest because it has a simple band structure with a single Dirac cone on the surface and a relatively large bulk gap (0.3 eV) among topological insulator materials.[2,3] In Bi_2Se_3, five covalently bonded atomic sheets (e.g., Se-Bi-Se-Bi-Se) compose one quintuple layer (QL, ∼1 nm).[4] Each QL is weakly bonded by van der Waals interactions which allow exfoliation into a few QLs.[5] Theoretical studies revealed that the conducting surface states are concentrated in a few QLs thicknesses.[6,7] Cui et al. demonstrated that the large surface-to-volume ratio of Bi_2Se_3 nanoribbons effectively suppresses the bulk effect and helps in probing the transport properties of the surface states.[4]

It was reported that the surface states of an epitaxially grown Bi_2Se_3 thin films are sensitive to the thickness. The conducting states of the top and bottom surfaces couple together and lead to an insulating state when the film is thinner than ∼5 QLs;[6,7] thus, thickness control can be an interesting variable, allowing adjustment of the energy gap from an insulator to a conductor.[7] Simple thinning to nanosheets can open a possibility of local confinement of electrons for quantum-information technologies. This unique property may be used to fabricate ultrathin field-effect transistors that are sensitive to gate voltages, thereby operating at an extremely low voltage.[8]

So far, Bi_2Se_3 nanosheets or nanoplates have been prepared mainly through vapor processes.[8,9] Despite recent success in synthesis of layered V−VI nanomaterials (Bi_2Se_3, Bi_2Te_3, Sb_2Te_3, etc.), most approaches suffer from slow reaction rate[10] or produce relatively thick plates with poorly defined morphology.[11,12] Zhang et al. recently presented a polyol process to generate Bi_2Se_3 hexagonal nanosheets of ∼4 QLs or thicker.[13] Their study focused on the physical states of the nanosheets, and the growth mechanism was not revealed. Clear understanding on the growth mechanism is critical to prepare ultrathin Bi_2Se_3 nanosheets with controlled uniformity and shape via an easily accessible solution process. Because the electronic states of the nanosheets are sensitively variable at <6 QLs, preparation of nanosheets with a few QLs is of specific interest. Massive production of epitaxially grown single-crystal Bi_2Se_3 nanosheets may pave a new way to generate large-area topological insulator thin films. We need a quick process to guarantee uniformity and quantitative production.

Here we suggest a simple and quick synthetic route to prepare ultrathin single-crystal Bi_2Se_3 nanodiscs and nanosheets with a typical thickness of 4−6 QLs. The growth mechanism, including self-attachment of small nanoparticles (NPs) and epitaxial recrystallization, is discussed in detail. We found the overall shape of the nanodiscs is sensitive to synthesis temperature and surfactants: high temperature produced nanodiscs with well-developed facets, and amine-containing surfactants greatly enlarged the lateral dimension, producing ultrathin nanosheets.

Figure 1 illustrates the crystal structure and the growth mechanism together with TEM images corresponding to each growth step. The anisotropic bonding caused by the weak van der Waals interaction between the QLs of Bi_2Se_3 intrinsically prefers 2D nanostructures such as nanodiscs or nanosheets.[9] A reaction batch (250 mL three-neck round-bottom flask) contained ethylene glycol (120 mL), Na_2SeO_3 (99%, Aldrich, 0.24 g), $Bi(NO_3)_3\cdot 5H_2O$ (99.99%, Aldrich, 0.45 g), and poly(vinylpyrollidone) (PVP) (M_w = 55 000, Aldrich, 1.0 g) as surfactant. The reaction was triggered by rapid injection of 22.4 mL of hydroxylamine solution (NH_2OH, 50% in H_2O, Aldrich, 2.4 mL in 20 mL of ethylene glycol) at 180 °C. To investigate the growth mechanism, small amount of the solution was transferred via pipet (2 mL) to a cold vial kept in an ice bath to quench the reaction. The products were

Received: October 24, 2011
Published: January 30, 2012

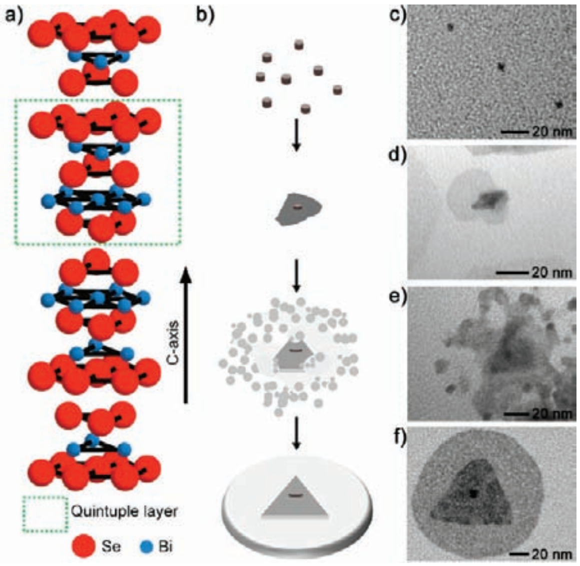

Figure 1. (a) Unit cell of rhombohedral crystal structure of Bi_2Se_3. Each QL consists of five consecutive atomic sheets (Se-Bi-Se-Bi-Se). (b) Scheme for the growth of a nanodisc from a nanocrystal, involving attachment of small NCs and recrystallization into a single-crystal nanodisc. A second layer grows epitaxially on the primary nanodisc. (c−f) TEM images corresponding to the growth steps in (b).

collected after at least 3 washing cycles. Experimental details are found in the Supporting Information.

After rapid injection of the reducing agent in the reaction medium at 180 °C, the temperature quickly dropped to 160 °C. Small crystals were nucleated within 5 s (Figure 1c) and grew further into larger crystals (Figure 1d). Small NPs were additionally generated after the temperature was restored to 180 °C. The additional NPs were attached to the seed crystals (Figure 1e), as suggested by previous studies.[14] A trianglular second layer evolved at the center of the nanodisc, indicating recrystallization of the attached NPs. The seed crystals were centered because of the burst random attachment of the NPs. Finally, the self-organized NPs formed a single-crystal nanodisc within 30 s (Figure 1f). At this stage, no seed crystals or particles were observed in TEM studies.

A TEM image (Figure 2a) shows attachment of the NPs to the edge of a growing seed crystal. The attached NPs are indicated by dotted red lines. At this stage, the attachment was not epitaxial, as seen in the inset image of the black circle in Figure 2a. Both experiments and simulations have shown that epitaxial reorientation can take place during annealing of randomly oriented particles. Epitaxial rearrangement is induced by relaxation of stress resulting from a misorientation at the attachment interface.[15] Due to the intrinsic preference for 2D growth, epitaxial rearrangement is considered to have a small energy barrier. It was often found even in small particle aggregations (Figure 2b). This growth mechanism is different from the ripening process which involves dissolution of small particles and re-deposition of the dissolved atoms to larger particles. Further annealing for 24 h at the reaction temperature did not change the shape, indicating the nanodiscs are thermodynamically stable in the solution.

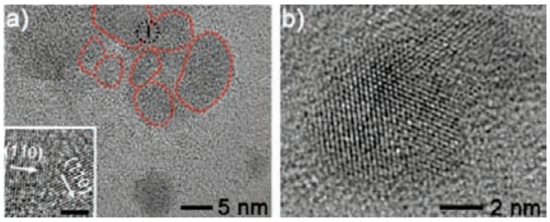

Figure 2. (a) TEM image showing attachment of Bi_2Se_3 NPs to the edge of an evolving nanodisc. The areas enclosed by dashed lines indicate the attached NPs. (b) HR-TEM image showing epitaxial reorientation between two isolated NPs.

The continuous attachment and fast epitaxial rearrangement are thermodynamically driven by the dependence of the surface charges on size. In layered Bi_2Se_3, the top layer is covered by Se atoms whose negative charges provide stability in polar solvents or in the presence of surfactants with positive charges. The other facets are neutralized or weakly charged because the charges from Se and Bi atoms compensate each other. When the particles are <5 nm (a few QLs thick), the effective charged area per mass is not prominent, and the zeta potential is not large enough to stabilize the particles in the reaction medium. They aggregate side-by-side to increase the surface along the [110] direction and epitaxially rearrange into a single crystal. The charged surface area increases as the reaction time increases. The zeta potential of the particles in 5 s was −15 mV (Figure S1). When they grew into nanodiscs in 30 s, it decreased to −40 mV, which is in a regime of stable dispersion. The dispersion character without the aid of surfactants can be a practical advantage in device fabrication.

Figure 3a shows a TEM image of the Bi_2Se_3 nanodiscs synthesized at 180 °C in the presence of PVP as surfactant. The nanodiscs had a good uniformity in size with an average lateral diameter of ~150 nm. Figure 3b shows a bilayered Bi_2Se_3 nanodisc. Figure 3c,d shows high-resolution TEM images of the center of the nanodisc and the end of the second layer, designated by letters c (solid circle) and d (dotted line) in Figure 3b. The central region reveals a hexagonal lattice fringe with a lattice spacing of 0.21 nm, consistent with the lattice spacing of the (110) plane. The selected area electron diffraction (SAED) in the inset confirmed the [001] zone axis. Figure 3d verifies the same lattice fringes between the first and the second layers. The SAED pattern in the inset clearly indicates epitaxial growth of the second layer. In a nonepitaxial manner, the crystal orientations along the (110) surface must be tilted between the two layers. AFM analysis reveals that the first layer of the nanodisc had a thickness of ~4 nm (Figure 3e), corresponding to a stack of 4 QLs. Any first layer showed the same thickness, while the triangular second layer had 2 or 4 QLs. Powder X-ray diffraction (XRD) confirmed the rhombohedral structure (a = 0.4139 nm, c = 2.8636 nm, JCPDS Card No. 33-0214) (Figure 3f). Vertical lines indicate the corresponding peaks of bulk Bi_2Se_3. Because the nanodiscs were stacked face-on on a flat substrate, (110) planes exhibited stronger intensity compared with those of bulk Bi_2Se_3. The elements of the Bi_2Se_3 nanodiscs were mapped by EDS (Figure 3g). Bi and Se were uniformly distributed with a stoichiometric composition of 2:3 atomic ratio (Figure S2). The small portion of C mainly originated from the carbon-coated copper grid for TEM anaylsis. Although nanodiscs with a triangular second layer were the major product in this process, circular nanodiscs without any secondary layer or with two additional layers were also found (Figure S3). The seed nanocrystals (NCs) were always centered. Nanodiscs without a second layer are expected to be made from a small seed NC, while nanodiscs with

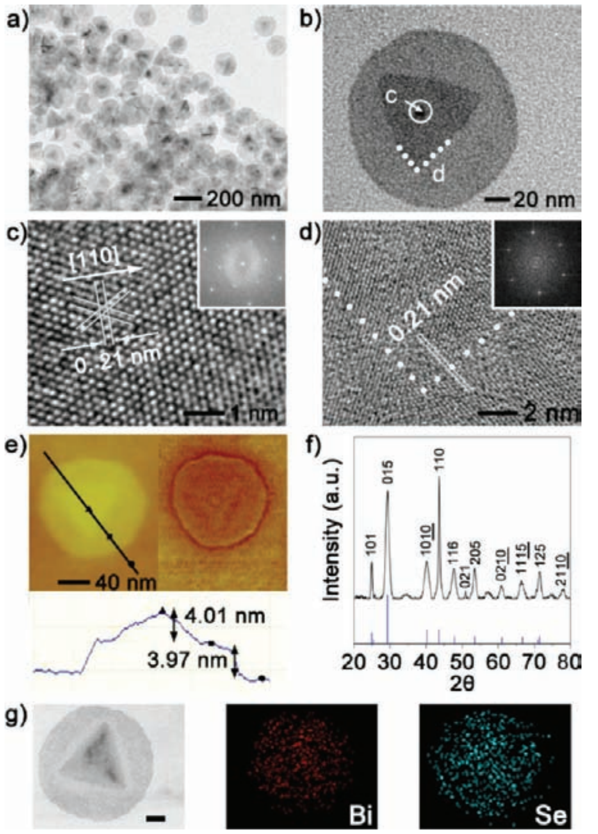

Figure 3. (a) TEM image of Bi_2Se_3 nanodiscs synthesized at 180 °C in the presence of PVP. (b) HR-TEM image of a Bi_2Se_3 nanodisc with a triangular secondary layer. (c,d) HR-TEM images of the areas designated by the letters c (solid circle) and d (dotted line) in panel b. The insets are SAED patterns. (e) AFM analysis of a bilayer Bi_2Se_3 nanodisc with 4 QLs thickness in each layer. (f) XRD analysis of Bi_2Se_3 nanodiscs. The peaks are indexed to the rhombohedral structure. (g) STEM image of a typical Bi_2Se_3 nanodisc and atomic distribution of Bi and Se atoms. Scale bar = 30 nm.

multiple layers can grow from large seed NCs. The growth of the second layer is considered to be restricted by the size of the bottom layer. The triangular shape of the second layer is natural because the Se atomic sheets of each QL have a 60° facet angle difference for epitaxial growth.[16]

Raman spectroscopy is sensitive to local atomic arrangements and vibrations of materials. The Raman spectrum of bulk Bi_2Se_3 exhibits four Brillouin zone center Raman active modes: 37, 72, 131, and 174 cm^{-1}, assigned as E_g^1, A_{1g}^1, E_g^2, and A_{1g}^2, respectively.[13,17] Figure S4 shows Raman spectra of the bulk and the nanodiscs. A monolayer of nanodiscs was prepared on a Si wafer by evaporating the solvent from a drop of the nanodisc suspension. Three peaks (A_{1g}^1, E_g^2, and A_{1g}^2) from the bulk Bi_2Se_3 were consistent with the literature. We found the A_{1g}^1 peak from the nanodiscs shifted (~3 cm^{-1}) to lower wavenumber, mainly because the out-of-plane vibration is less restrained in the nanodiscs than in the bulk.[13,18]

In the synthesis, reaction temperature was critical to the growth and shape of the Bi_2Se_3 nanodiscs. Figure 4 shows the effect of reaction temperature on the shape and size. At 100 °C, small NPs with irregular shapes (~50 nm diameter) were produced (Figure 4a,b). At 140 °C, the products grew into nanodiscs with an average diameter of ~100 nm, but the structure of the second layer was not fully developed (Figure 4c,d). At 200 °C with the same reaction conditions, well-defined hexagonal nanodiscs with a truncated triangular second layer were the major product (Figure 4e,f). The diameter of the nanodiscs increased to ~180 nm. Nanodiscs without a second layer and with multiple layers were also found (see Figure S5). High reaction temperature is regarded to facilitate burst formation of seed particles and rapid growth of nuclei into nanodiscs, enhancing the size-uniformity of the nanodiscs. AFM analysis revealed that the first and second layers of nanodiscs synthesized at 200 °C consist of 4 QLs and 2 QLs, respectively (Figure S6). XRD spectra of Bi_2Se_3 nanodiscs synthesized at different reaction temperatures were indexed to the rhombohedral crystal structure (Figure S7).

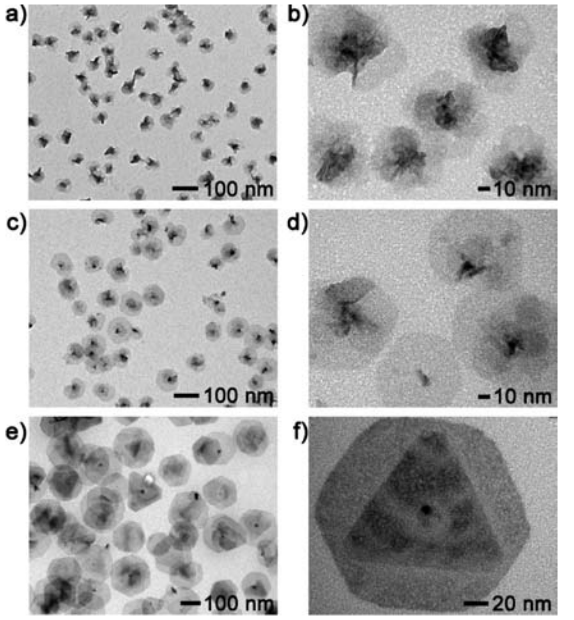

Figure 4. TEM images of Bi_2Se_3 synthesized in the presence of PVP at 100 (a,b), 140 (c,d), and 200 °C (e,f).

Surfactants also had a critical impact on the final morphology of the nanodiscs. In the absence of any surfactant, each nanodisc had a short second nanodisc emerging vertically from the plane perpendicular to the c-axis at its center (Figure S8). Due to the negative charges at the surface, surfactants with negative charges played no role in the structure determination or surface stability of the products. For example, poly(acrylic acid) (M_w = 450 000, Aldrich), a typical negatively charged surfactant, did not protect the plane perpendicular to the c-axis, so it produced flower-like structures consisting of many nanodiscs (Figure S8). Regardless of the surfactant, the crystal structure of Bi_2Se_3 was rhombohedral (Figure S8).

Meanwhile, poly(ethylene imine) (PEI, M_w = 25 000, Aldrich), a representative positively charged surfactant, effectively stabilized the plane perpendicular to the c-axis and hindered growth along the *c*-axis. PVP, the most frequently used surfactant, contains tertiary amine and carbonyl; thus, binding to the negatively charged surface by the amine groups is weaker than that by the primary amine in PEI. We examined the charge effect of the surfactants by adjusting the molar ratio of PVP and PEI at 180 °C. Figure 5 shows the results at mixing ratios of 9:1, 8:2, 3:7, and 0:1. Addition of a small amount of PEI (Figure 5a) enlarged the lateral dimension of the nanodiscs to ~250 nm diameter. The second layers were smaller than the primary layer; therefore, their shape was not necessarily triangular. At PVP/PEI = 80:20, the lateral dimension of the

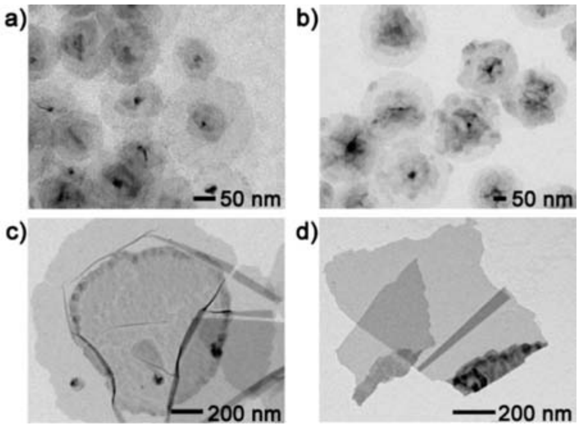

Figure 5. TEM images of Bi_2Se_3 nanodiscs and nanosheets synthesized at different mixing ratios of PVP and PEI as surfactants. Weight ratios (PVP/PEI): (a) 9:1, (b) 8:2, (c) 3:7, and (d) 0:1.

disc-like shape increased to ~350 nm diameter. Additional NCs were continuously attached to the growing nanodiscs, so multiple layers were frequently observed on the nanodiscs (Figure 5b). Figure S9 shows magnified TEM images of typical nanodiscs synthesized using mixing ratios of 9:1 and 8:2.

When PEI was the majority surfactant (Figure 5c), the disc-like shape was seldom observed. Instead, the lateral dimension of the nanosheets was further extended to a few micrometers. When we used only PEI as surfactant, the nanosheets laterally grew to a large dimension. The reaction is extremely fast; the particle size should be uniform and limited unless the surface potential of the particles is extremely small. The negative charges of Se atoms cannot be completely screened by PVP; thus, limited growth of nanodiscs in PVP surfactant is reasonable. In contrast, PEI can effectively screen the surface charges, making negligible the increase in surface potential by attachment of small NPs. Therefore, the driving force of NP attachment is much larger. The ultrathin nanosheets were crumpled during solvent evaporation. They were readily torn apart by applying mild ultrasonic sound (Figure 5d). Since the nanosheets were severely crumpled (Figure S10), they could not stack face-on on a flat substrate by simple drying (Figure S10). The XRD pattern resembled that of bulk Bi_2Se_3 (Figure S10). At any mixing ratio, the resulting nanodiscs and nanosheets typically had thicknesses of 4 and 6 QLs (Figure S11). These results suggest that PVP mainly controlled the shape determination and size uniformity by restricting the growth of nanodiscs because the weak binding limits the decrease in surface energy of the growing nanodiscs. Meanwhile, PEI fostered continuous lateral growth of the nanosheets by effectively reducing the surface energy of the plane perpendicular to the c-axis.

In summary, single-crystal ultrathin Bi_2Se_3 nanodiscs and nanosheets were successfully synthesized. The growth was enabled by consecutive 2D attachment of nanocrystals and epitaxial recrystallization. The intrinsic preference for a layered structure with negatively charged Se atoms was the driving force of self-organization. Upon raising the reaction temperature, the lateral dimension of the nanodiscs was extended, and the shape changed from circular to hexagonal discs. Addition of positively charged surfactants largely extended the lateral dimension of the nanosheets with 4−6 QLs thickness.

■ ASSOCIATED CONTENT

Ⓢ Supporting Information

Experimental details and analytical data. This material is available free of charge via the Internet at http://pubs.acs.org.

■ AUTHOR INFORMATION

Corresponding Author

ujeong@yonsei.ac.kr

Author Contributions

[§]These authors contributed equally.

Notes

The authors declare no competing financial interest.

■ ACKNOWLEDGMENTS

This research was supported by a National Research Foundation grant funded by the Korean Government through the World Class University Program (R32-20031), Korea Research Foundation (KRF-2007-311-D00367), and Fusion Research Program for Green Technologies (2011-0000004).

■ REFERENCES

(1) Bernevig, B. A.; Hughes, T. L.; Zhang, S. C. *Science* **2006**, *314*, 1757.

(2) Zhang, H.; Liu, C.-X.; Qi, X.-L.; Dai, X.; Fang, Z.; Zhang, S.-C. *Nat. Phys.* **2009**, *5*, 438.

(3) Xia, Y.; Qian, D.; Hsieh, D.; Wray, L.; Pal, A.; Lin, H.; Bansil, A.; Grauer, D.; Hor, Y. S.; Cava, R. J.; Hasan, M. Z. *Nat. Phys.* **2009**, *5*, 398.

(4) Peng, H.; Lai, K.; Kong, D.; Meister, S.; Chen, Y.; Qi, X.-L.; Zhang, S.-C.; Shen, Z.-X.; Cui, Y. *Nat. Mater.* **2010**, *9*, 225.

(5) Hong, S. S.; Kundhikanjana, W.; Cha, J. J.; Lai, K.; Kong, D.; Meister, S.; Kelly, M. A.; Shen, Z.-X.; Cui, Y. *Nano Lett.* **2010**, *10*, 3118.

(6) Cho, S.; Butch, N. P.; Paglione, J.; Fuhrer, M. S. *Nano Lett.* **2011**, *11*, 1925.

(7) Zhang, Y.; He, K.; Chang, C.-Z.; Song, C.-L.; Wang, L.-L.; Chen, X.; Jia, J.-F.; Fang, Z.; Dai, X.; Shan, W.-Y.; Shen, S.-Q.; Niu, Q.; Qi, X.-L.; Zhang, S.-C.; Ma, X.-C.; Xue, Q.-K. *Nat. Phys.* **2010**, *6*, 584.

(8) Kong, D.; Dang, W.; Cha, J. J.; Li, H.; Meister, S.; Peng, H.; Liu, Z.; Cui, Y. *Nano Lett.* **2010**, *10*, 2245. Zhang, G.; Qin, H.; Chen, J.; He, X.; Lu, L.; Li, Y.; Wu, K. *Adv. Funct. Mater.* **2011**, *21*, 2351.

(9) Bayaz, A. A.; Giani, A.; Artaud, M. C.; Foucaran, F.; Pascal-Delannoy, F.; Boyer, A. *J. Cryst. Growth* **2002**, *241*, 463. Dang, W.; Peng, H.; Li, H.; Wang, P.; Liu, Z. *Nano Lett.* **2010**, *10*, 2870.

(10) Scheele, M.; Oeschler, N.; Veremchuk, L.; Reinsberg, K.-G.; Kreuziger, A.-M.; Kornowski, A.; Broekaert, J.; Klinke, C.; Weller, H. *ACS Nano* **2010**, *7*, 4283.

(11) Wang, W.; Poudel, B.; Yang, J.; Wang, D. Z.; Ren, Z. F. *J. Am. Chem. Soc.* **2005**, *127*, 13792. Shi, W.; Zhou, L.; Song, S.; Yang, J.; Zhang, H. *Adv. Mater.* **2008**, *20*, 1892.

(12) Zhou, B.; Ji, Y.; Yang, Y.-F.; Li, X.-H.; Zhu, J.-J. *Cryst. Growth Des.* **2008**, *8*, 4394.

(13) Zhang, J.; Peng, Z.; Soni, A.; Zhao, Y.; Xiong, Y.; Peng, B.; Wang, J.; Dresselhaus, M. S.; Xiong, Q. *Nano Lett.* **2011**, *11*, 2407.

(14) Tang, Z.; Zhang, Z.; Wang, Y.; Glotzer, S. C.; Kotov, N. A. *Science* **2006**, *314*, 274. Yu, T.; Lim, B.; Xia, Y. *Angew. Chem., Int. Ed.* **2010**, *49*, 4484.

(15) Yeadon, M.; Ghaly, M.; Yang, J. C.; Averback, R. S.; Gibson, J. M. *Appl. Phys. Lett.* **1998**, *73*, 3208.

(16) Zhang, G.; Qin, H.; Teng, J.; Guo, J.; Guo, Q.; Dai, X.; Fang, Z.; Wu, K. *Appl. Phys. Lett.* **2009**, *95*, 053114.

(17) Richter, W.; Kohler, H.; Becker, C. R. *Phys. Status Solidi B* **1997**, *84*, 619.

(18) Shahil, K. M. F.; Hossain, M. Z.; Teweldebrhan, D.; Balandin, A. A. *Appl. Phys. Lett.* **2010**, *96*, 153103.